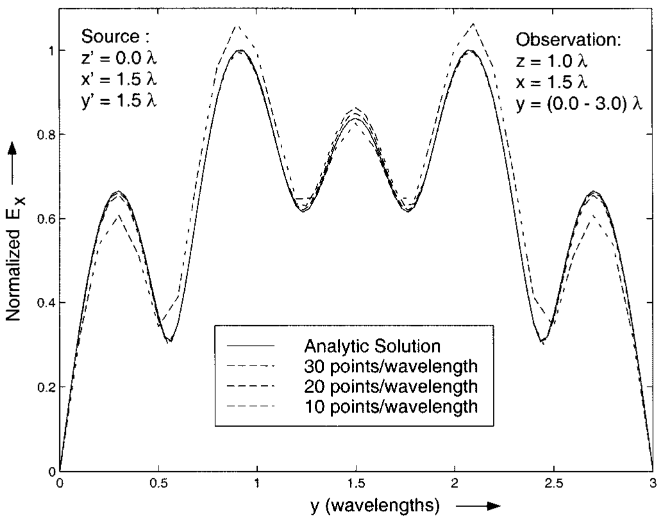

Fig. 3. Point source response for a square waveguide of size $3\lambda \times 3\lambda$ at different discretization levels.

the first few propagating modes of the channel waveguide are shown in Fig. 2.

To test the accuracy of the localized current source response, we compared our results for a homogeneously filled square waveguide with the analytic solution. A square waveguide of size $3\lambda \times 3\lambda$ was discretized at three different levels (10, 20, and 30 points/λ). A point current source was placed at the center of the waveguide and the field was computed at a distance of 1λ from the source. Fig. 3 plots the field along the y-axis center cut for the different discretization levels and compares them with the analytic solution obtained using the dyadic Green's function for a rectangular waveguide. The results are not very good when just ten points per wavelength are used and get worse as the wave is propagated down the waveguide. However, at a grid density of 30 points per wavelength, excellent agreement is seen with the analytic solution.

VI. Conclusions

We have developed an algorithm to solve the eigenvalue problem for the sparse matrix generated by the finite-difference formulation. The use of bi-Lanczos algorithm allows this method to be computationally competitive with other approximate methods, while the use of the finite-difference formulation makes this method versatile enough to handle complicated waveguide structures. We have also described a new technique that reduces the storage requirements to $O(N)$ and, thus, allows us to solve problems with several 100 000 unknowns. We have also described a scheme to solve for the localized current source response using an extension of the SLDM technique.

References

[1] W. Schlosser and H. G. Unger, "Partially filled waveguides and surface waveguides of rectangular cross-section," in *Advances in Microwaves*. New York: Academic, 1966.

[2] J. E. Goell, "A circular-harmonic computer analysis of rectangular dielectric waveguide," *Bell Syst. Tech. J.*, vol. 48, pp. 2133–2160, 1969.

[3] B. M. A. Rahman and J. B. Davies, "Finite-element analysis of optical and microwave waveguide problems," *IEEE Trans. Microwave Theory Tech.*, vol. MTT-32, pp. 20–28, Jan. 1984.

[4] W. C. Chew and M. Nasir, "A variational analysis of anisotropic, inhomogeneous dielectric waveguides," *IEEE Trans. Microwave Theory Tech.*, vol. 37, p. 661, Apr. 1989.

[5] E. Schweig and W. B. Bridges, "Computer analysis of dielectric waveguides: A finite-difference method," *IEEE Trans. Microwave Theory Tech.*, vol. MTT-32, pp. 531–541, May 1984.

[6] K. Bierwirth, N. Schulz, and F. Arndt, "Finite-difference analysis of rectangular dielectric waveguide structures," *IEEE Trans. Microwave Theory Tech.*, vol. MTT-34, pp. 1104–1114, Nov. 1986.

[7] N. Schulz, K. Bierwirth, F. Arndt, and U. Köster, "Finite-difference method without spurious solutions for the hybrid-mode analysis of diffused channel waveguides," *IEEE Trans. Microwave Theory Tech.*, vol. 38, pp. 722–729, June 1990.

[8] A. T. Galick, T. Kerkhoven, and U. Ravaioli, "Iterative solution of the eigenvalue problem for a dielectric waveguide," *IEEE Trans. Microwave Theory Tech.*, vol. 40, pp. 699–705, Apr. 1992.

[9] W. C. Chew, "Electromagnetic theory on a lattice," *J. Appl. Phys.*, vol. 75, pp. 4843–4850, May 1994.

[10] G. H. Golub and C. F. Loan, *Matrix Computations*. Baltimore, MD: The Johns Hopkins Univ. Press, 1989.

[11] H. I. van der Veen, "Eigenproblem algorithms for large and sparse nonsymmetric matrices," TNO, Rijswijk, The Netherlands, Rep. 93-NM-R1260, 1993.

[12] V. Druskin and L. Knizhnerman, "Two polynomial methods of calculating functions of symmetric matrices," *U.S.S.R. Comput. Math. Math. Phys.*, vol. 29, no. 6, pp. 112–121, 1989. (Russian: translated into English).

A Low-Power-Consuming SOM for Wireless Communications

M. Ghanevati and A. S. Daryoush

***Abstract*—This paper presents theoretical and experimental results of a low-power-consuming hybrid push–pull self-oscillating mixer (SOM) circuit at the UHF frequency band. The frequency-stable SOM circuit is designed and fabricated using matched-pair Si bipolar junction transistors and high-Q resonators, where measured phase noise of this free-running voltage-controlled oscillator is -101.2 dBc/Hz at 100-kHz offset. A 20-dB up-conversion gain, a compression dynamic range (CDR) of 65 dB · MHz, and a spurious-free dynamic range of 50 dB · MHz$^{2/3}$ are also measured for the mixer portion of this SOM. Moreover, a down-conversion gain of ≈ -2 dB with a CDR of 100 dB · MHz is also measured.**

***Index Terms*—Low phase-noise oscillator, nonlinear modeling, push–pull amplifier, self-oscillating mixer, Si BJT, UHF.**

I. Introduction

Low-power-consuming front-end electronic circuits are important elements in future mobile communication systems [1]. Self-oscillating mixer (SOM) circuits that combine both local oscillators (LOs) and mixer functions have found interests in RF transceivers since they exhibit a smaller size and potentially a lower overall power consumption [2]–[7] as opposed to their discrete counter parts. A low-power-consuming SOM design topology based on the push–pull concept was first demonstrated at X-band [7] and was later modified and extended to the

Manuscript received October 5, 1999.

M. Ghanevati was with the Department of Electrical and Computer Engineering, Microwave Photonics Device Laboratory, Drexel University, Philadelphia, PA 19104 USA. He is now with Boeing Satellite Systems, El Segundo, CA 90245 USA (e-mail: Manouchehr.Ghanevati@Boeing.com).

A. S. Daryoush is with the Department of Electrical and Computer Engineering, Microwave Photonics Device Laboratory, Drexel University, Philadelphia, PA 19104 USA (e-mail: daryoush@ece.drexel.edu).

Publisher Item Identifier S 0018-9480(01)05055-4.

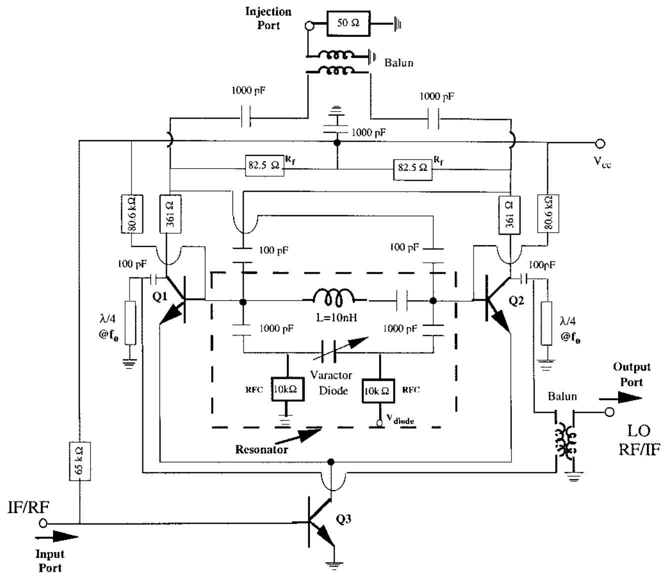

Fig. 1. Schematic diagram of the SOM for UHF frequencies.

wireless communications applications using input and output baluns [8].

Since the LO signal in the design concepts of [6]–[9] is inherently unstable, injection-locked and phase-locked loop (ILPLL) approach [10] is employed to frequency stabilize the free-running oscillators. For example, the design approach of [8] lacks adequate LO stability and suffers from a high pulling factor due to its low Q factor; hence, injection locking was used for its frequency stabilization. This paper presents a hybrid circuit that is realized in the push–pull topology that is similar to a multifunction monolithic microwave integrated circuit (MMIC) [9] demonstrated for clock recovery applications. We propose this circuit for implementation of a low-cost antenna front-end electronics, where the power-efficient up- and down-converter of IF and RF signals with stable LOs is useful. More specifically, this paper presents design, simulation, realization, and experimental results of a multifunction SOM circuit that exhibits excellent frequency stability, low power consumption, and efficient up- and down-conversion characteristics. However, even though preliminary experimental results of this circuit were reported in [11], more detailed theoretical and experimental results of the modified circuit are provided in this paper.

II. Design Approach

The proposed SOM circuit is based on the push–pull differential amplifier operating in class AB as a gain block [7]–[9], as shown in Fig. 1. A push–pull concept is effective when the matched pair transistors and components are used in the circuit, which makes this design most suitable for MMIC realization. For a hybrid prototype realization, matched-pair Si bipolar junction transistors (BJTs) from Bipolarics (SOIC-8 plastic package part BTA105M2) are characterized and their nonlinear Gummel–Poon SPICE model parameters are extracted for design optimization (cf. [12] for the extraction procedure). As depicted in Fig. 1, the feedback resistors R_f sample the collector current in transistor $Q1$ ($Q2$) and provide a positive feedback voltage to the base of transistor $Q2$ ($Q1$). Thus, the bases of both transistors are 180° out-of-phase due to the coupling between the collector of $Q1$ ($Q2$) with the base of $Q2$ ($Q1$). The class-AB push–pull amplifier provides high gain as long as this 180° phase condition is satisfied. This phase condition necessary for push–pull amplification is destroyed at all frequencies, except at the resonant frequency of the resonant tank circuit.

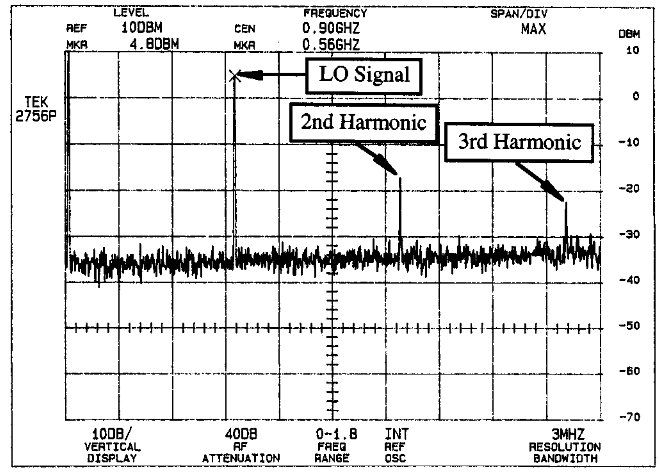

Fig. 2. Measured power spectrum of the free-running oscillator at 560 MHz. The marker shows a signal level of about 5 dBm at 560 MHz. Second and third harmonics are also shown.

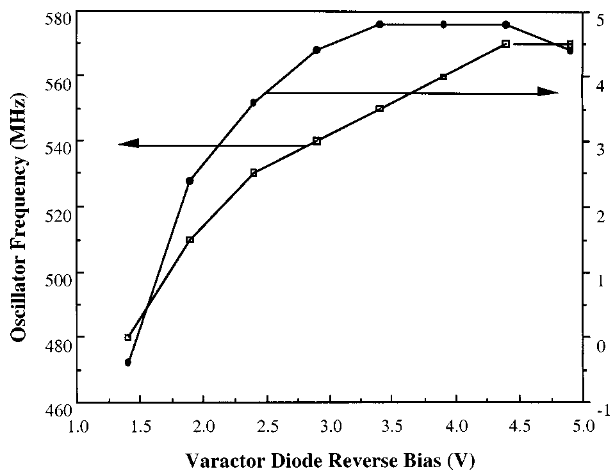

Fig. 3. Measured oscillation frequency and power level versus varactor diode's reverse bias voltage.

Thus, the oscillation frequency is established by the resonance condition of the parallel resonator circuit, where the resonator behaves like an open circuit, thus isolating the bases of transistors $Q1$ and $Q2$. Away from the resonance condition, the 180° phase shift between the base voltages of transistors $Q1$ and $Q2$ is destroyed and the push–pull amplification condition is not satisfied. A 10-nH inductor from Coilcraft with a Q of 85 at 900 MHz (part 0603HS-10NTJBC) is used in the resonant tank circuit. Frequency tuning of the oscillator is achieved by tuning the resonant frequency of the parallel resonance circuit using a high-Q hyper-abrupt varactor diode from Alpha Industries, Woburn, MA. 10-kΩ resistors have been used as RF choke as part of dc biasing of the varactor diode.

To achieve a low phase-noise oscillation signal, quarter-wavelength short-circuited resonators from SMI, Osaka, Japan, are used across the collector of transistors $Q1$ and $Q2$. These small sizes ($\varepsilon_r = 90$) and high-Q coaxial resonators (measured $Q_{ex} = 220$) enhance the overall oscillator performance and filter out any spurious oscillation frequencies. Furthermore, the high-Q resonators help the speed in which oscillation starts by increasing the overall frequency selectivity of the push–pull amplifier. The presence of these resonators also helps reduce the level of the even-order harmonics of the LO at the output port. The large internal oscillation signal combined with the high circuit nonlinearity of the push–pull topology provides an efficient mixing in this

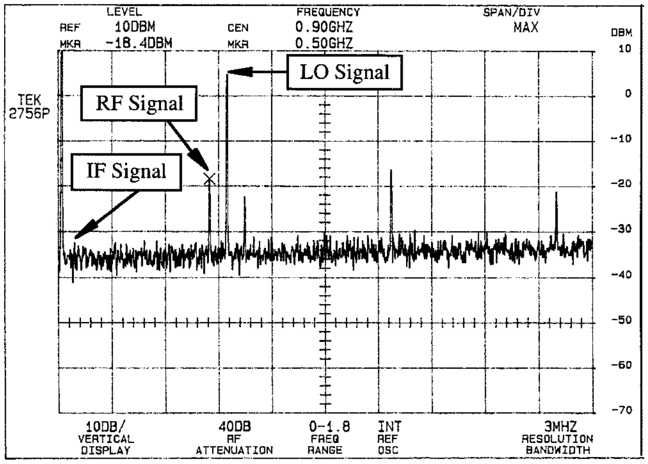

Fig. 4. Measured power spectrum of the SOM in the case of IF signal up-conversion. The IF signal is at 60 MHz at −40-dBm input power. (Vertical scale of 10 dB/div span of max, resolution bandwidth of 3 MHz.)

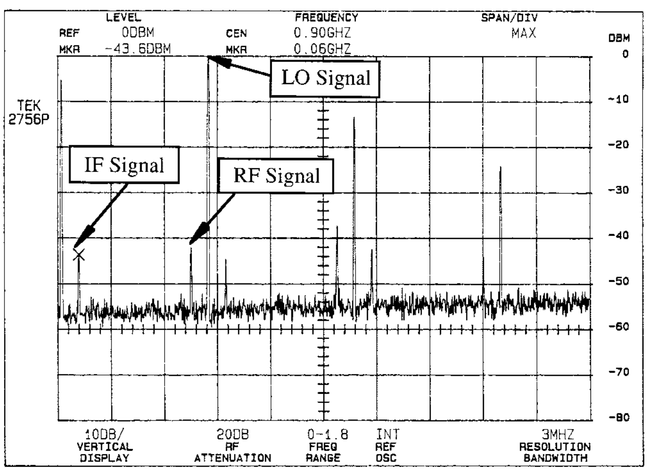

Fig. 5. Measured power spectra of the SOM in the case of IF signal down-conversion. The RF signal is at 440 MHz with −40 dBm input power. (Vertical scale of 10 dB/div, span of max, and resolution bandwidth of 3 MHz.)

SOM. The input IF (RF) signal can be applied to the base of a micro-x plastic package transistor $Q3$ (Bipolarics part B12V105) for mixing with the LO signal, resulting in the RF (IF) signal at the output port.

A single-ended output has been provided by means of a 4 : 1 Guanella balun. The balun has been designed and fabricated using 36-gauge wire on a low-loss ferrite bead using a 4 : 1 ratio transformer. The balun performance is also fitted to an equivalent-circuit model. To provide for the option of achieving even higher frequency stability, an additional port is also provided to force oscillation to follow spectral purity characteristics of a reference signal using the injection-locking process. To maintain the design symmetry in the SOM circuit and to provide proper impedance matching, the injected signal is fed through a balun. In addition to a single-ended output circuit shown in Fig. 1, a circuit with two balanced output ports (not shown in Fig. 1) have been implemented for direct integration with external components (e.g., a buffer amplifier) mounted on printed circuit boards. These outputs, however, have not been utilized in this experimentation.

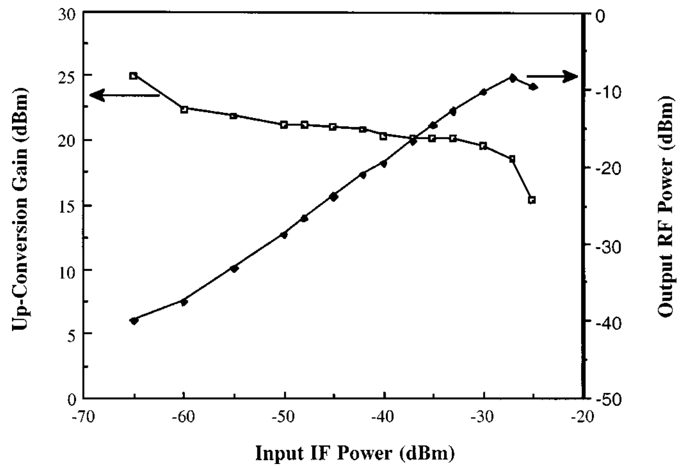

Fig. 6. Measured RF output power and up-conversion gain versus input IF power.

III. Simulation and Experimental Results

A hybrid version of this SOM is designed, simulated, and fabricated on FR4 substrate with a measured relative dielectric constant of 4.25 and a thickness of 29 mil. All the lumped components and active devices are surface-mount components and their equivalent-circuit models are fully developed to accurately simulate this SOM. The nonlinear SPICE parameters for both BJT packaged transistors (i.e., BTA105M2 and B124105) have been extracted and an excellent match between the measured and simulated dc I–V curves have been achieved. Furthermore, the extracted nonlinear parameters and package parasitic have been successfully verified through full two-port S-parameter measurements at various classes of operation (cf. [12]). The SOM performance is simulated using a commercial nonlinear microwave computer-aided design (CAD). The class-AB operation of $Q1$ and $Q2$ with the transistor $Q3$ as a current source consumes only 38-mW power using a 5-V-battery supply. The measured and simulated bias current values for the circuits agree very closely. The measured results also indicate a closely matched operation for the differential transistor pairs $Q1$ and $Q2$. Both simulated and measured results indicate that as a result of the external coaxial resonators, the oscillation starts at a faster rate with higher output power with a lower close-in to carrier phase noise compared to earlier topologies [7], [8].

Experimental results associated with the oscillator portion of the SOM are first reported. The power spectrum for the measured free-running oscillator is depicted in Fig. 2. This figure depicts the first three harmonics of the free-running oscillator at 560 MHz. These results generally match with the corresponding harmonic-balance (HB) simulator results of 1.85, −24.2, and −18.5 dBm. The difference is primarily due to the loading effect of the injection port used in the HB simulator. Although the injection port shown in Fig. 1 was implemented in the prototype circuit, it was not utilized for stabilization of the oscillator due to its low incidental FM noise.

The measured close-in to carrier phase noise at offset frequencies of 10 and 100 kHz are −80 and −101 dBc/Hz, respectively. However, the injection port could be used to achieve even further frequency stability. By changing the varactor diode reverse bias from 1.4 to 4.4 V, the frequency of oscillation is tuned from 480 to 570 MHz without any adverse FM noise degradation or power variation, as depicted in Fig. 3.

TABLE I
HB SIMULATION RESULTS FOR THE UP/DOWN MIXING OF THE SOM

Mixing	f_{LO}(MHz) / Power Level (dBm)	f_{IF}(MHZ) / Power Level (dBm)	f_{RF}(MHz) / Power Level (dBm)	Conversion Gain (dB)
UP-Conversion IF_{in}@-40 dBm	560 / 1.85	60 / -45.4	500 / -21.6	18
Down-Conversion RF_{in}@-40dBm	500 / 2.3	60 / -38.2	440 / -26.8	2

Note a linear frequency tuning with a sensitivity of 20 MHz/V at varactor diode reverse bias of about 3.5 V.

Next, mixing characteristics of this SOM are reported. Both the up- and down-conversion are measured as a function of input IF and RF power. The measured power spectrum of the up-converted IF signal at 500 MHz for an input IF signal at 60 MHz is depicted in Fig. 4. The simulated plot obtained from HB simulator (not shown here) predicts an up-conversion gain of about 18 dB versus the measured gain of 20 dB. The above results are very close. The measured power spectrum of the down-converted RF signal at 60 MHz for an input RF signal at 440 MHz is depicted in Fig. 5, indicating a gain of -2 dB. The down-conversion mixing gain is suffered as a result of using external coaxial resonators at the output of the SOM circuit. Moreover, a strong LO signal is present at the output. The LO signal can be removed for the down-conversion case using a low-pass filter. However, in the case of up-conversion, a high-order filter is required to separate LO and RF and design of small-size bandpass filter is a challenge.

The simulated conversion gain is about 2 dB. Table I summarizes the simulated values for up- and down-conversion mixing of the SOM using an HB simulator (Series IV), where the predicted results, in general, matches with the measured results. The measured output RF power and up-conversion gain versus input IF power is depicted in Fig. 6. The corresponding plot for the down-conversion mixing is reported in [12]. The simulated results also show strong presence of an LO signal.

Intermodulation distortion (IMD) measurement was also performed on the up-converted mixer. The measured 1-dB compression point and the intercept point (IP-3) are -27 and -2 dBm, respectively. The measured noise figure of this SOM is about 1.9 dB. A compression dynamic range (CDR) of 65 dB $\cdot$ MHz and a spurious-free dynamic range of 50 dB $\cdot$ MHz$^{2/3}$ were obtained from measurement for a 1-MHz receiver bandwidth.

IV. CONCLUSIONS

An SOM topology is reported in this paper that operates with high-conversion gain at UHF frequency bands. In addition to its high-conversion gain, this SOM topology exhibits an extremely low power consumption and low close-in to carrier phase noise. However even though, for further frequency stabilization, injection locking ports are incorporated in the design, it was not exploited due to its excellent frequency stability. The proposed design topology is attractive for antenna front-end transceiver modules in use by many handheld mobile communication units, such as pagers, smart cards, and wireless modems. Moreover, this topology is suitable as an integral part of clock recovery circuits for high-throughput encoding protocol (e.g., 8B 10B and S-20) with speeds as high as 10 Gb/s. The only disadvantage of this SOM circuit as a mixer appears to be is its low RF/LO isolation, which can be improved with proper filtering.

ACKNOWLEDGMENT

The authors would like to thank R. Gutierrez, Stellex-Phoenix Microwave, San Jose, CA, for his technical suggestions and support in fabrication of the SOM circuit.

REFERENCES

[1] "Special Issue on Low-Power RF Systems," *Proc. IEEE*, vol. 88, Oct. 2000.
[2] Y. Tajima, "GaAs FET applications for injection-locked oscillators and self-oscillating mixers," *IEEE Trans. Microwave Theory Tech.*, vol. MTT-27, pp. 629–632, July 1979.
[3] R. Stahlmann, C. Tsironis, F. Ponse, and H. Beneking, "Dual-gate MESFET self-oscillating X-band mixers," *Electron. Lett.*, vol. 15, no. 17, pp. 524–526, Aug. 1979.
[4] C. Tsironis, "12 GHz receiver with self-oscillating dual-gate MESFET mixer," *Electron. Lett.*, vol. 17, pp. 617–618, 1981.
[5] V. D. Hwang and T. Itoh, "Quasi-optical HEMT and MESFET self-oscillating mixers," *IEEE Trans. Microwave Theory Tech.*, vol. 36, pp. 1701–1705, Dec. 1988.
[6] I. Kipnis and A. Khanna, "Large-signal computer-aided analysis and design of silicon bipolar MMIC oscillator and self-oscillating mixers," *IEEE Trans. Microwave Theory Tech.*, vol. 37, pp. 558–564, Mar. 1989.
[7] X. Zhou and A. S. Daryoush, "An efficient self-oscillating mixer for communications," *IEEE Trans. Microwave Theory Tech.*, vol. 42, pp. 1858–1862, Oct. 1994.
[8] A. V. Thangavelu, H. P. Moyer, M. Ghanevati, A. S. Daryoush, and R. Gutierrez, "Push–pull frequency converter for mobile communication," in *IEEE MTT-S Int. Microwave Symp. Dig.*, vol. 2, Denver, CO, 1997, pp. 661–664.
[9] A. S. Daryoush, X. Zhang, and J. Y. Lin, "1/4 W optical receiver and clock recovery circuit for Gb/s digital fiberoptic links," in *IEEE MTT-S Int. Microwave Symp. Dig.*, vol. 2, San Francisco, CA, 1996, pp. 891–894.
[10] D. J. Sturzebecher, X. Zhou, X. Zhang, and A. S. Daryoush, "Optically controlled oscillators for millimeter-wave phased array antennas," *IEEE Trans. Microwave Theory Tech.*, vol. 41, pp. 998–1004, June–July 1993.
[11] M. Ghanevati, A. V. Thangavelu, J. H. Lee, R. Gutierrez, and A. S. Daryoush, "An efficient SOM for front-end UHF electronics," in *IEEE MTT-S Int. Microwave Symp. Dig.*, vol. 4, Anaheim, CA, 1999, pp. 1769–1772.
[12] M. Ghanevati, "Active antennas with an efficient multifunction self-oscillating mixer for wireless communications," Ph.D. dissertation, Elect. Comput. Eng. Dept., Drexel Univ., Philadelphia, PA, June 1999.